

Indentation mechanics and fracture behavior of metal/ceramic nanolaminate composites

N. Chawla · D. R. P. Singh · Y.-L. Shen ·
G. Tang · K. K. Chawla

Received: 18 November 2007 / Accepted: 4 January 2008 / Published online: 18 April 2008
© Springer Science+Business Media, LLC 2008

Abstract Composite laminates on the nanoscale have unique properties, such as high strength, high wear resistance, and biocompatibility. In this paper we report on the nanoindentation behavior of a model metal–ceramic nanolaminate consisting of alternating layers of aluminum and silicon carbide (Al/SiC) processed by PVD on a Si substrate. Composites with different layer thicknesses were fabricated and the effect of layer thickness on Young’s modulus and hardness was quantified. The effect of indentation depth on modulus and hardness was studied. The damage that took place during nanoindentation was examined by cross-sectioning the samples by focused ion beam (FIB) technique and imaging the surface using scanning electron microscopy (SEM). Finite element modeling (FEM) of nanoindentation of nanolaminates was conducted. The damage patterns observed in experiments were qualitatively supported by the numerical simulations.

Introduction

Synthetic and natural composite laminates have been shown to exhibit a combination of excellent strength and toughness [1]. Composite laminates on the nanoscale with

unique properties, such as high strength, high wear resistance, and biocompatibility have been developed. These composites have been investigated in many different layered combinations: Metal–metal composites [2–4], metal–ceramic composites [5–10], and ceramic–ceramic composites [11, 12]. Metal–ceramic nanolaminate systems can exhibit a combination of high strength and toughness. Mechanical and microstructural characterization of these composites are important. Because the composites are on the nanoscale, obtaining and understanding their mechanical properties is also a challenge. Nanoindentation has been used extensively to extract Young’s modulus and hardness of nanolaminates. A fundamental understanding of how these nanolaminates behave under indentation loading is still lacking. In particular, several important issues need to be addressed:

1. The stress state under the indenter in monolithic materials is complex. This stress state is even more complex in metal–ceramic nanolaminates because of the intrinsic heterogeneity introduced by alternating hard and soft layers.
2. Most of these composites are made by physical vapor deposition (PVD) on a substrate, such as Si. The mechanical properties are a function of indentation depth, thus, the contribution of the substrate increases with depth.
3. Because of the large and complex state of stress under the indenter, damage during the indentation process will take place. The precise nature and evolution of damage in these composites are not well understood.

In this paper we have studied the nanoindentation behavior of a model metal–ceramic nanolaminate consisting of alternating layers of aluminum and silicon carbide (Al/SiC) processed by PVD on a Si substrate. Composites with

N. Chawla (✉) · D. R. P. Singh
School of Materials, Fulton School of Engineering, Arizona
State University, Tempe, AZ 85287-8706, USA
e-mail: nchawla@asu.edu

Y.-L. Shen · G. Tang
Department of Mechanical Engineering, University of New
Mexico, Albuquerque, NM, USA

K. K. Chawla
Department of Materials Science and Engineering, University
of Alabama at Birmingham, Birmingham, AL 35294, USA

different layer thicknesses were fabricated and the effect of layer thickness on Young's modulus and hardness was quantified. The effect of indentation depth on modulus and hardness was studied. The damage that took place during nanoindentation was examined by cross-sectioning the samples using a focused ion beam (FIB) technique and imaging the surface using scanning electron microscopy (SEM). Finite element modeling (FEM) of nanoindentation of nanolaminates was done. It will be shown that the FEM model qualitatively explains the experimentally observed behavior.

Materials and experimental procedure

The nanolaminated composites were fabricated by magnetron sputtering of Al and SiC. The multilayers were grown on a single crystal silicon (111) substrate. The sputter unit consisted of a high vacuum chamber with dual sputter guns. The base pressure of the sputtering chamber was approximately 10^{-7} Torr (1.33×10^{-7} Pa). Targets of pure Al (99.99%) and SiC (99.5%) (Kurt Lesker, Clairton, PA) were used for sputtering in argon atmosphere, at an argon pressure of about 3 mTorr (0.4 Pa). Al was sputtered using a DC sputter gun with a power of 95 W while SiC was sputtered by a RF sputter gun at 215 W. The targets were pre-sputtered for about 10 min at 40 W for Al and 95 W for SiC to remove any oxides and impurities from the surface. Under these conditions, the deposition rates were approximately 7.5 nm/min for Al and 3.9 nm/min for SiC [9]. During deposition the sample holder was continuously rotated to obtain uniform thickness of film on the substrate. Two multilayered samples were grown and analyzed, one with Al and SiC layers of about 50 nm each, and the other with Al and SiC layers of about 25 nm each. A total of 41 alternating layers (21 Al and 20 SiC) were grown to obtain a relatively thick sample for nanoindentation (with reduced effects of the substrate [13]).

The microstructure of the nanolaminates was characterized using a dual beam FIB with a Field Emission Gun

SEM (FEI, Nova 200 NanoLab). FIB offers versatility in micromachining of a variety of materials. It was particularly suitable in this study because the nanolaminates consisted of alternating hard and soft layers. In our laminates, a flat surface would not be achieved using conventional polishing techniques. The samples were cross-sectioned along the thickness to measure layer thicknesses of the sputtered samples, as well as to evaluate the damage after nanoindentation. A thin platinum layer was deposited on the sample prior to FIB machining to minimize ion beam damage. A Ga^+ ion source was used for milling the surface at a voltage of 30 kV. For rough milling of a "trench," a beam current of 1 nA was used. The final cleaning cross-sections were conducted at a much smaller beam current (10 pA).

Nanoindentation was conducted using a commercial nanoindenter (Nano-XP, MTS Systems, Minneapolis, MN). The indenter was calibrated using a fused silica standard. At least 20 indentations were made on each of the samples. The continuous stiffness measurement (CSM) technique was employed during nanoindentation to measure Young's modulus and hardness as a function of displacement. This technique consists of a superimposed small harmonic force over the load. The contact stiffness is continuously measured from the phase and amplitude shifts of the output signal. Details of the CSM technique are given elsewhere [14].

Results and discussion

Microstructure characterization

Two multilayered structures with different Al and SiC thicknesses were processed using magnetron sputtering. The cross-sections of the nanolaminates, obtained by FIB, are shown in Fig. 1. The layer thicknesses were measured from the images and are shown in Table 1. The first multilayered nanolaminate had Al and SiC thickness of around 58 and 45 nm, respectively, while the second nanolaminate

Fig. 1 Scanning electron micrographs of Al/SiC multilayers cross-sectioned by focused ion beam (FIB): (a) Al₅₀SiC₅₀ (Al layer thickness of 58 nm and SiC layer thickness of 45 nm) and (b) Al₂₅SiC₂₅ (Al layer thickness of 27 nm and SiC layer thickness of 18 nm)

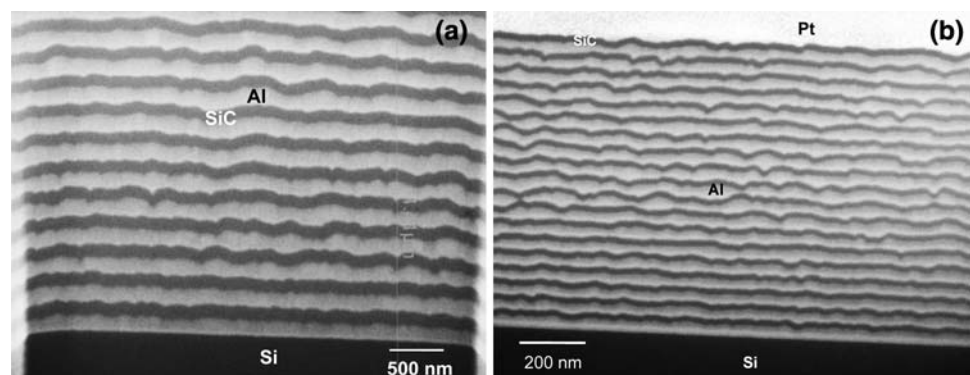


Table 1 Individual thickness and SiC volume fraction in Al/SiC nanolaminated composites

Composite laminate	Al thickness (nm)	SiC thickness (nm)	Volume fraction of SiC (%)	Total laminate thickness (μm)
Al50SiC50	58 ± 3	45 ± 3	43.7	~2
Al25SiC25	27 ± 2	18 ± 1	40.0	~1

had thicknesses of 27 and 18 nm, respectively. We designate these two composites as Al50SiC50 and Al25SiC25. The variability in layer thickness was relatively small, and the volume fraction of SiC in both multilayers was kept constant at around 40%. Each composite had 41 layers, with Al being both the first and last layer in the composites. Thus, the Al50SiC50 composite with thicker layers had a total thickness of 2 μm, while Al25SiC25 composite with the thinner layers had a total thickness of 1 μm. Some degree of roughness in both Al and SiC, due to the columnar growth morphology of Al, was observed. The SiC layer roughness follows that of the previous Al layer.

Nanoindentation

Young’s modulus and hardness of the multilayers, measured by nanoindentation, are presented in this section. The properties were measured using the CSM technique, so the evolution of modulus and hardness was obtained instantaneously as a function of indentation depth. Representative load versus displacement and modulus versus displacement curves, as a function of indentation depth, are shown in Fig. 2a. Figure 2b shows a magnified view of the initial indentation process. In the first 20–50 nm of penetration, the modulus is relatively low. Here the indenter is probing only the first Al layer, with some contribution from the underlying SiC layer as well as other layers. Young’s modulus of the multilayered laminate appears to stabilize

and is relatively constant over the displacement range of 100–200 nm. This is indicative of a Young’s modulus representative of the overall composite, as the indenter displacement is at a depth of least four to five layers. The limited contribution from the substrate at shallow depths (<10% of the multilayer thickness) has also been observed in other systems [15]. With increasing indentation depth, the modulus begins to increase, as a function of an increased contribution from the Si substrate. At larger depths the contribution from the Si substrate appears to be offset by the onset of damage in the form of SiC fracture and void growth in the Al layers, which causes a decrease in the modulus. Finally, at very large depths (1,600–1,700 nm) a pronounced discontinuity in the load-displacement curve is observed. This can be attributed to damage at the multilayer–Si substrate interface and within the Si substrate itself. A more detailed description of the damage mechanisms is provided in the next section. Representative modulus and hardness versus displacement curves, for both composites, are shown in Fig. 3. A comparison of the modulus and hardness of both Al50SiC50 and Al25SiC25 multilayers is shown in Table 2. The modulus was taken at about 10% of the total composite thickness, to minimize any substrate effects. As expected, the modulus of the two composites was similar since the modulus is controlled by the volume fraction of the two phases and is less dependent on individual layer thickness. The evolution of the hardness did not exhibit a plateau region with increasing displacement. Thus, we arbitrarily compare the hardness over the displacement range of 100–200 nm. Note that this displacement range is still within 20% of the composite thickness. The hardness data obtained should still be representative of the composite considered here, according to earlier studies on the hardness–displacement relationship in thin film/substrate systems [16, 17]. The hardness was significantly affected by layer thickness. In metallic multilayered composites, decreasing layer thickness also significantly increases the

Fig. 2 (a) Load versus displacement curve from nanoindentation of Al50SiC50 composite. The evolution of Young’s modulus with indentation displacement is shown. (b) Magnified view of the early part of the indentation process. After indentation of the first Al layer, a plateau commensurate with Young’s modulus of the overall composite is observed

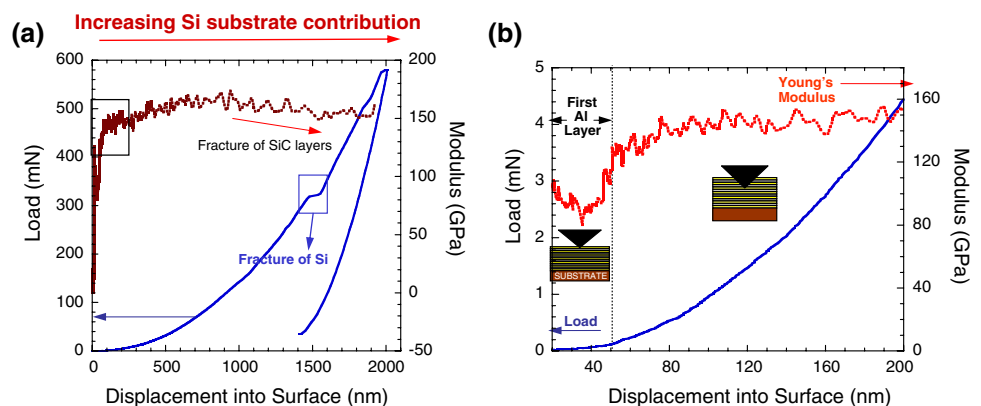


Fig. 3 Comparison of (a) Young's modulus and (b) hardness for Al50SiC50 and Al25SiC25 composites. Young's modulus is not affected by layer thickness, as it is controlled by the volume fraction of the phases. Hardness is affected by layer thickness, as the plastic deformation of the Al layers is more constrained at the smaller thickness

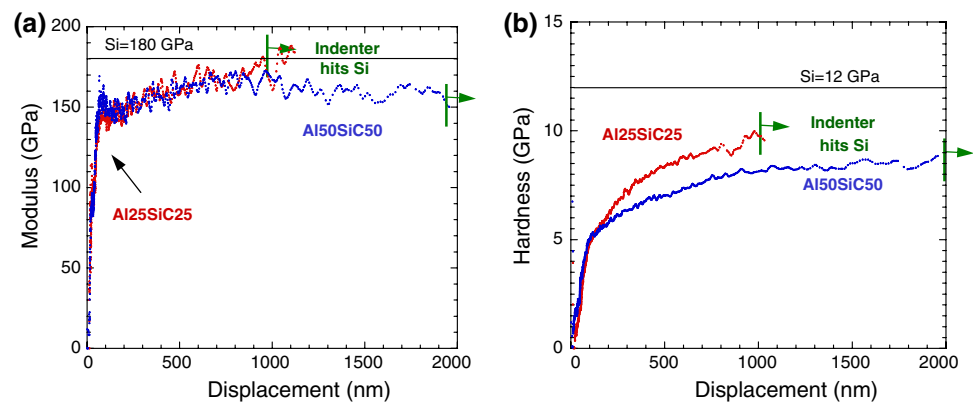


Table 2 Modulus and hardness of the two multilayer samples as measured from nanoindentation

Material	Modulus (GPa)	Displacement range for modulus (nm)	Hardness (GPa)	Displacement range for hardness (nm)
Al (1,000 nm) (after Deng et al. [9])	60 ± 23	60–110	0.68 ± 0.09	100–200
SiC (1,000 nm) (after Deng et al. [9])	277 ± 11	40–80	25.9 ± 0.9	100–200
Al50SiC50	148 ± 8	100–200	4.8 ± 0.7	100–200
Al25SiC25	141 ± 12	50–100	6.4 ± 0.5	100–200

hardness of the multilayered composite [18]. In our study, the SiC layers serve to constrain the plastic deformation in the Al layers, thereby increasing the hardness of the composite.

Damage mechanisms and fractography

Characterization of damage during indentation was conducted by cross-sectional analysis using the FIB and SEM. The process used to prepare cross-section surfaces suitable for analysis is shown in Fig. 4. A Pt layer was deposited over the composite to minimize beam damage. This was

followed by milling a wide trench in the region of interest at a high beam current (30 nA). A fair amount of beam damage was introduced at this current. The region of interest was then “polished” with a much smaller beam current (10 pA) to resolve the microstructure. The damage processes presented here are restricted to the Al50SiC50 samples. Indentations at depths of 1,000 and 2,000 nm were analyzed.

Figure 5 shows a cross-section near the center of an indentation at a depth of 1,000 nm. Note that cracking in the SiC layers is clearly visible. The cracks appear to take place due to a local shear band. The cracks appeared to

Fig. 4 Cross-sectioning and imaging of damage under an indentation using the FIB-SEM: (a) indentation, (b) platinum layer deposited on the indentation to minimize beam damage, (c) trench milled at high ion beam current (30 nA) (d) surface after fine milling/polishing at low beam current (10 pA)

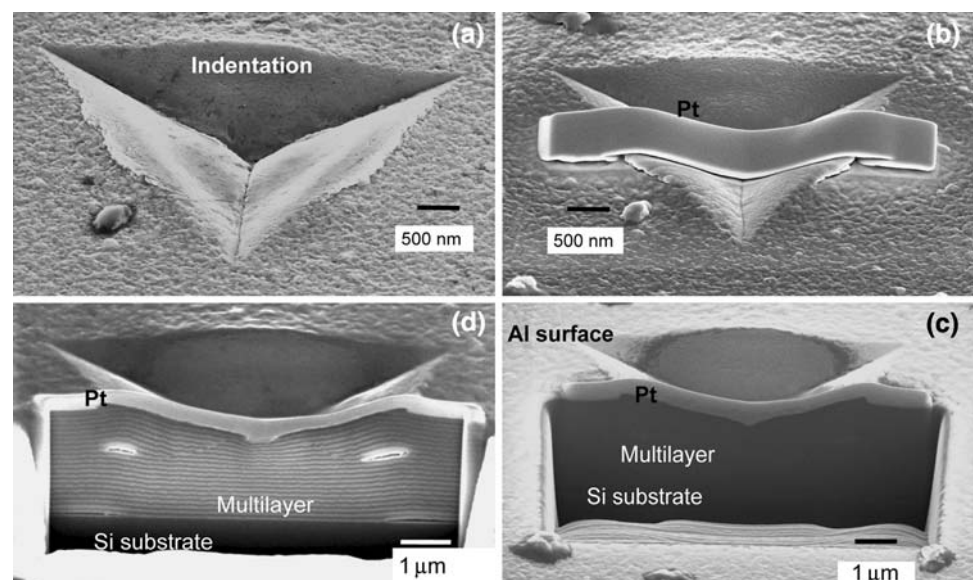
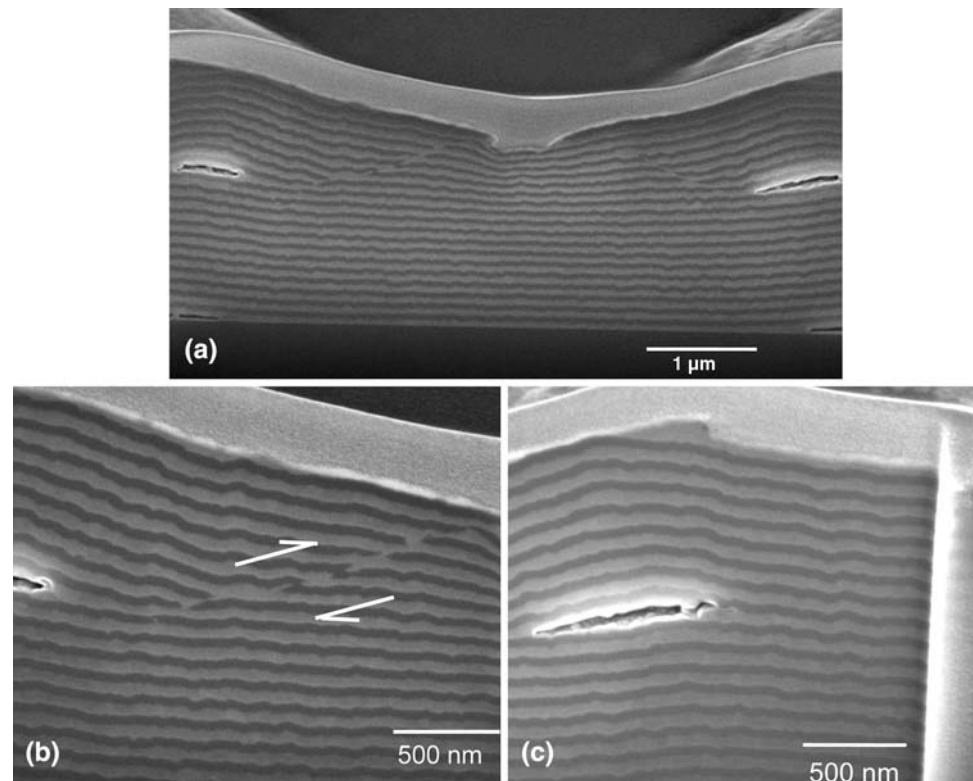


Fig. 5 (a) FIB cross-section of an indentation at a depth of 1,000 nm, (b) high magnification of SiC cracking at a shear band, and (c) void growth within an Al layer



have been filled with the plastic flow of Al from the Al layers. Voids within the Al layers, near the indenter edges were also observed. It is important to note that the voids do not occur at the interface of Al and SiC. Rather, the voids grow within the Al layer. This suggests that the strength of the Al/SiC interface is higher than the stress required for void formation in the Al layer. The voids appear in a region below the piled-up region of the indentation and may be a result of tensile stress generated by the constraint from brittle SiC layers locally during indentation. Void growth can also be observed in the first Al layer on the Si substrate.

A cross-section of the indentation at 2,000 nm is shown in Fig. 6. Note multiple shear zones and fracture of SiC in multiple planes. An important feature that can be seen is the flexibility of the SiC layers. Near the piled-up regions the SiC layers have been deformed to a very small radius of curvature, in some cases without fracturing (Fig. 6). The large degree of flexibility of the SiC layers is enhanced by the large amount of plasticity afforded by the Al layers that sandwich the SiC layers. A more quantitative understanding of the flexibility of the SiC layers can be obtained by using an analogy of a simple beam in bending. Here the ratio of bending moment, M , to the moment of inertia, I , is given by [19, 20]:

$$\frac{M}{I} = \frac{E}{R} \quad \text{and} \quad MR = EI$$

where E is Young's modulus and R is the radius of curvature. The quantity MR is called flexural rigidity. One

thus defines the inverse of flexural rigidity, $1/MR$, as a measure of flexibility. For a beam of rectangular cross-section, the moment of inertia, I is equal to $bh^3/12$, where b is equal to the width and h the height or thickness of the beam. Thus, the flexibility in a given SiC layer can be written as:

$$\frac{1}{MR} = \frac{12}{Ebh^3}$$

The significance of the above result is that the flexibility of the layer goes as h^{-3} , so that, at the nanoscale the layers should be expected to have extremely high flexibility. This has profound and important implications for designing tough and flexible multilayered materials. Finally, even though the indenter did not penetrate the substrate, significant substrate deformation and fracture occurred in the Si substrate at 2,000 nm (see Fig. 6c). Note that fracture appears primarily within the Si substrate, although limited delamination at the substrate Al interface is also observed.

Modeling

To qualitatively explain the experimentally observed damage behavior during nanoindentation, finite element analysis was conducted. It was based on an axisymmetric model of 41 layers of alternating Al and SiC layers above the Si substrate, as schematically shown in Fig. 7. The

Fig. 6 (a) FIB cross-section of an indentation at a depth of 2,000 nm showing multiple shear bands and SiC cracking, (b) high magnification of large degree of flexibility of SiC and microcracking, and (c) delamination at the multilayer/Si interface and fracture within Si

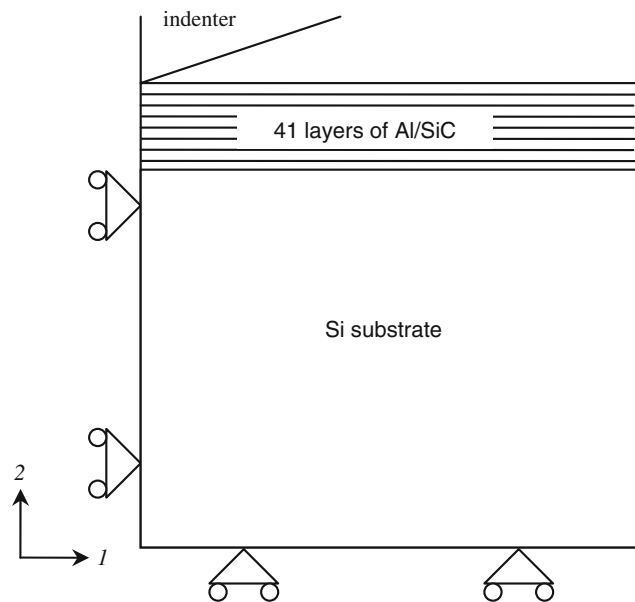
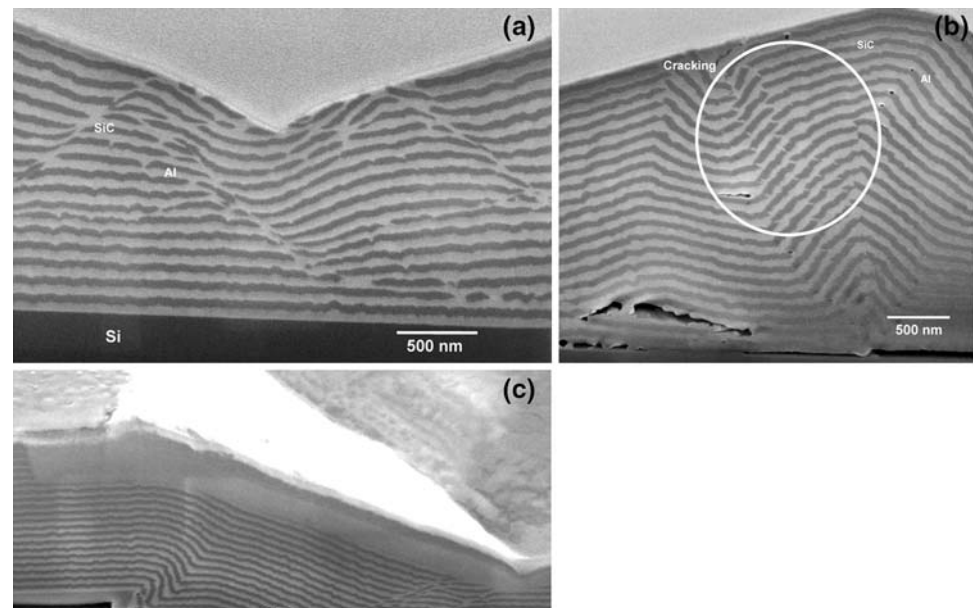
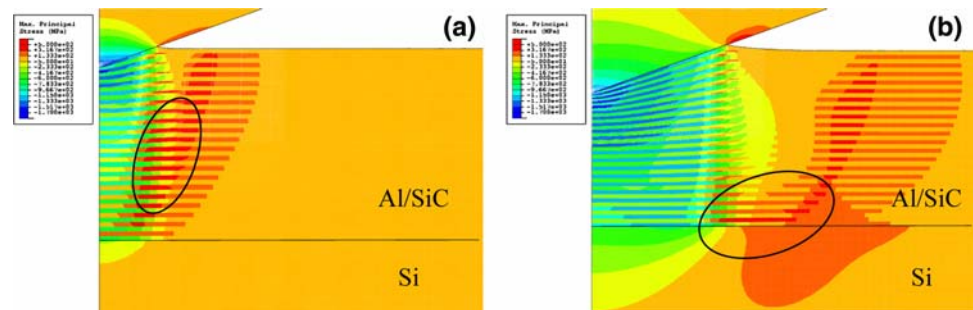


Fig. 7 Schematic showing the composite model and the boundary conditions for the nanoindentation modeling. The specimen and indenter both possess axial symmetry about the left boundary. The rigid indenter has a semi-angle of 70.3°

left boundary is treated as the symmetry axis. The semi-angle of the conical elastic diamond indenter is 70.3° , resulting in the same projected area as that of a Berkovich indenter [21]. The overall size of the entire specimen is taken as $40\ \mu\text{m}$ in lateral span (radius) and $43\ \mu\text{m}$ in height. Each Al and SiC layer is 50-nm thick. During deformation the left boundary is allowed to move only in the 2-direction. The bottom boundary is allowed to move

only in the 1-direction. The right boundary is not constrained. The part of top boundary not under indentation is also free to move. When contact with the indenter is established, the surface portion engaged by the indenter is restricted to follow the indenter contour. The finite element program ABAQUS (Version 6.5, Dassault Systemes Simulia Corp., Providence, RI) was employed. A total of 173,105 axisymmetric four-noded linear elements (order of integration 2×2) were used in the model, with a finer mesh size near the upper-left corner. Both Al and SiC were taken to be simple continua having an isotropic elastic–plastic response. In the actual material the SiC layers were amorphous and the Al layers had a columnar polycrystalline structure. Al is known to possess a high degree of isotropy. Therefore, for the purpose of obtaining a representative indentation stress field to qualitatively explain the observed damage, the simple continuum-based approach is considered adequate. The input Young’s moduli for Al and SiC were 59 and 277 GPa, respectively, which were measured experimentally using nanoindentation on single-layer Al and SiC films. Poisson’s ratios for Al and SiC were taken to be 0.33 and 0.17, respectively. The plastic response of Al was based on the tensile loading data of single-layer Al [9], with an initial yield strength 200 MPa. Two stages of linear strain hardening were used: 200 MPa up to a plastic strain of 0.5 and then 40 MPa up to a plastic strain of 3.0. To improve computational efficiency, the model used an “apparent” SiC plastic flow strength which is five times that of Al. The simulation is thus able to offer useful qualitative insight on damage location while avoiding the potential numerical problem when attempting to indent

Fig. 8 Contours of maximum principal stress near the indentation site, when the indentation displacement is at (a) 200 and (b) 500 nm. Some regions of high tensile stresses are highlighted



extremely hard layers to a sufficient depth. Young's modulus and Poisson's ratio of the diamond indenter were 1,141 GPa and 0.07, respectively. The interaction between the indenter and top-layer Al was simulated by the surface-based contact algorithm with finite sliding provided by ABAQUS. The classical isotropic Coulomb friction model was employed. The coefficient of friction at the contact is taken to be 0.1, which is a typical value for the diamond/metal contact pair [22, 23]. All interfaces between Al and SiC were assumed to be perfectly bonded so the displacement field across the interface is continuous. The automatic time step scheme featured in ABAQUS was selected, which is based on the maximum force residuals following each numerical iteration [24]. The finite element implementation is identical to a previous study on indentation modeling of metal/metal composite layers [25]. In the present simulation, no numerical convergence problem was encountered up to an indentation depth of 16 initial layer thicknesses.

Although a very large pressure exists underneath the indenter, significant local tensile stresses along certain directions can still be generated. Figure 8a and b shows the contour plots of maximum principal stresses when the indentation displacement reaches 200 and 500 nm, respectively. The Al/SiC layered structure can be discerned in areas where a large contrast in stress exists between the soft and hard layers. When the indentation displacement is relatively small, high tensile stresses can be seen in the mid-level SiC layers as highlighted in Fig. 8a. Further examinations of the numerical results (not shown) revealed that the high tensile stresses in this region are largely along the 1-direction. As a consequence, the tendency for brittle fracture in the SiC layers can be expected. As the indentation goes deeper, the stress field evolves into a different pattern. In Fig. 8b, high tensile stresses in SiC appear in the lower layers and toward the outer region. A part of the multilayer/substrate interface region is also under high tensile stresses as highlighted. The evolution of local stress field obtained from the model correlates well with some of the experimental observations shown in Figs. 5 and 6, especially the cracking in SiC layers and Si substrate.

Conclusions

The microstructure and indentation mechanics of metal-ceramic nanolaminated composites were examined. Based on our study, the following conclusions can be made:

- Nanoscale Al-SiC laminated composites of relatively large thickness were fabricated successfully.
- Multilayers with thinner individual layers had a higher hardness, because of a greater plastic constraint on the individual Al layers. Young's modulus was not affected by individual layer thickness, as it is controlled merely by the relative volume fractions of the two phases.
- Multilayers at the nanoscale exhibited significant flexibility during nanoindentation. Extensive pile-up observed in multilayers can be attributed to SiC layer bending and to plasticity in Al layers.
- Analysis by FIB showed that damage took place by localized cracking of SiC and plasticity and void nucleation and growth in aluminum layers. The voids were confined to the Al layers, indicating that the interface strength between Al-SiC and Al-Si substrate was higher than that of the fracture strength of Al.
- The damage pattern observed in experiments is qualitatively supported by the numerical simulations. High tensile stresses were found to exist in certain regions, which can be responsible for the cracking in SiC layers and Si substrate during the indentation process.

Acknowledgements The authors are grateful for financial support for this research from the National Science Foundation (DMR-0504781, Dr. H. D. Chopra, Program Manager). We acknowledge the use of processing and microscopy facilities at the LeRoy Eyring Center for Solid State Science at Arizona State University.

References

1. Lesuer DR, Syn CK, Sherby OD, Wadsworth J, Lewandowski JJ, Hunt WH (1996) *Int Mater Rev* 41:169
2. Huang H, Spaepen F (2000) *Acta Mater* 48:3261
3. Daniel C, Lasagni A, Mucklich F (2004) *Surf Coat Technol* 180–181:478

4. Schumann J, Brückner W, Heinrich A (1993) *Thin Solid Films* 228:44
5. Alpas AT, Embury JD, Hardwick DA, Springer RW (1990) *J Mater Sci* 25:1603. doi:[10.1007/BF01045357](https://doi.org/10.1007/BF01045357)
6. Mearini GT, Hoffman RW (1993) *J Electron Mater* 22(6):623
7. Chou TC, Nieh TG, McAdams SD, Pharr GM, Oliver WC (1992) *J Mater Res* 7(10):2774
8. Liu CH, Li W-Z, Li H-D (1996) *J Mater Res* 11(9):2231
9. Deng X, Chawla N, Chawla K, Koopman M, Chu JP (2005) *Adv Eng Mater* 7:1099
10. Deng X, Cleveland C, Karcher T, Koopman M, Chawla N, Chawla KK (2005) *J Mater Eng Perform* 14:417
11. Barshilia HC, Prakash MS, Poojari A, Rajan KS (2004) *Thin Solid Films* 460:133
12. Kuo D-H, Tzeng K-H (2004) *Thin Solid Films* 460:327
13. Saha R, Nix W (2002) *Acta Mater* 50:23
14. Li X, Bhushan B (2002) *Mater Charact* 48:11
15. Fischer-Cripps A (2000) *Vacuum* 58:569
16. Nix WD (1997) *Mater Sci Eng A* 234–A236:37
17. Tsui TY, Pharr GM (1999) *J Mater Res* 14:292
18. Misra A, Kung H (2001) *Adv Eng Mater* 3:217
19. Dresher WH (1969) *J Met* 21:17
20. Chawla KK (1998) *Fibrous materials*. Cambridge University Press, Cambridge, p 24
21. Fischer-Cripps AC (2002) *Nanoindentation*. Springer, New York, p 20
22. Lide DR (1995) *Handbook of chemistry and physics*, 76th edn. CRC Press, Boca Raton
23. Bucaille JL, Stauss S, Schwaller P, Michler J (2004) *Thin Solid Films* 447:239
24. ABAQUS Theory Manual, Version 6.5. Dassault Systemes Simulia Corp., Providence (2006)
25. Tan XH, Shen Y-L (2005) *Compos Sci Technol* 65:1639